Fresh properties of limestone-calcined clay-slag cement pastes

Chen, Yu; Zhang, Yu; Šavija, Branko; Copuroglu, Oguzhan

DOI
10.1016/j.cemconcomp.2023.104962

Publication date
2023

Document Version
Final published version

Published in
Cement and Concrete Composites

Cement and Concrete Composites 138 (2023) 104962

Contents lists available at ScienceDirect

Cement and Concrete Composites

journal homepage: www.elsevier.com/locate/cemconcomp

Fresh properties of limestone-calcined clay-slag cement pastes

Yu Chen *, Yu Zhang, Branko Šavija, Oğuzhan Çopuroğlu

Microlab, Faculty of Civil Engineering and Geosciences, Delft University of Technology, Delft, the Netherlands

ARTICLE INFO

Keywords:
Limestone and calcined clay
Slag
Fresh-state behaviors
Rheology
Water retention
Hydration
Compressive strength

ABSTRACT

Formulation of quaternary blended system containing ordinary Portland cement or clinker, slag, limestone and calcined clay (LC2) appeared to be a viable approach to developing low-clinker cements without severely sacrificing mechanical performance at later ages. This paper investigates the effect of two material parameters, i.e., LC2-to-slag ratio and gypsum content, on fresh properties, hydration, and compressive strength of quaternary blended cement pastes (about 65 wt% of LC2 and slag in the binder). Results show that the increase in LC2 proportion decreased flowability and increased water retention capacity, yield stress, and plastic viscosity, as well as accelerated the evolution of stiffness with time (G' growth). On the other hand, the addition of 2–4 wt% gypsum had little effect on most of the fresh properties. A new metric, the free water indicator, was proposed to describe the effect of free water content and the total specific surface area of binding materials. It correlated strongly with the growth of structural build-up metrics. Finally, adding gypsum delayed the aluminate peak and enhanced compressive strength only at 3 days, whereas increasing slag content reduced accumulated heat of hydration (7 days) but improved 28-day compressive strength. Therefore, adjusting LC2-to-slag ratio of the quaternary blended cement is a feasible way to meet requirements for fresh properties and compressive strength.

1. Introduction

In order to reduce the carbon footprint of the cement industry, growing attention has been given to the development and use of blended cements consisting of ordinary Portland cement (OPC) or clinker and supplementary cementitious materials (SCMs) [1,2]. Blast furnace slag (henceforth slag), as a byproduct of pig iron, is one of the most common SCMs for blended cements [3,4]. According to EN 197–1 [5], 36–95 wt% of clinker can be substituted with slag for formulating European CEM III cements. However, the total amount of slag available worldwide is only about 5–10% of the OPC produced. Moreover, considering environmental pressures, less iron is produced due to increased steel recycling [6]. Other common SCMs, i.e., fly ash and silica fume, have the same issue [6–8].

As an alternative to common SCMs, limestone and calcined clay (LC2) have been highlighted and have attracted great interest, considering their abundant deposits, sufficient supply worldwide, and low CO_2 emissions during production [6,9]. Limestone-calcined clay-cement (LC3) is believed to be one of the most promising alternatives for sustainable and high-performance cements [10]. The main reactive phase in calcined clay is calcined kaolinitic clay (metakaolin) that is rich in reactive silicate and aluminate. These reactive phases can react with calcium hydroxide (CH) from clinker hydration to form calcium-aluminosilicate-hydrate (C-A-S-H) and aluminate hydrates. The presence of calcite can also promote the formation of hemi/mono-carboaluminate by reacting with aluminate species (from C_3A and/or calcined clay) and CH in the pore solution. All these reactions contribute to the reduction of total porosity, enhancing the mechanical performance and durability of hardened cementitious materials [6,11,12]. The most typical ternary blend, LC3-50 (50 wt% clinker, 15 wt% limestone, 30 wt% calcined clay, and 5 wt% gypsum), displays comparable compressive strength with OPC after 7 days, and has already been adopted in industry trials in Cuba and India [6].

Unlike slag cements (CEM III/B–C cements), it is challenging to develop LC3 with a high content of LC2 (>50 wt%) without severely sacrificing the mechanical performance of hardened cementitious materials at later ages (after 28 days). Considerable decrease in compressive strength when replacing more than 50 wt% of OPC with LC2 has been reported [13]. The decrease in OPC content can dilute the alite hydration and weaken the pozzolanic reaction due to the reduction of CH formation. As Wang et al. [14] reported, formulation of quaternary blended system containing slag, OPC or clinker, and LC2 appeared to be a viable approach to developing low-clinker cements. The authors [14] found that LC2 promotes early-age hydration (within 7 days), and slag

* Corresponding author.
E-mail addresses: Y.Chen-6@tudelft.nl (Y. Chen), Y.Zhang-28@tudelft.nl (Y. Zhang), B.Savija@tudelft.nl (B. Šavija), O.Copuroglu@tudelft.nl (O. Çopuroğlu).

https://doi.org/10.1016/j.cemconcomp.2023.104962
Received 22 October 2022; Received in revised form 14 January 2023; Accepted 27 January 2023
Available online 2 February 2023

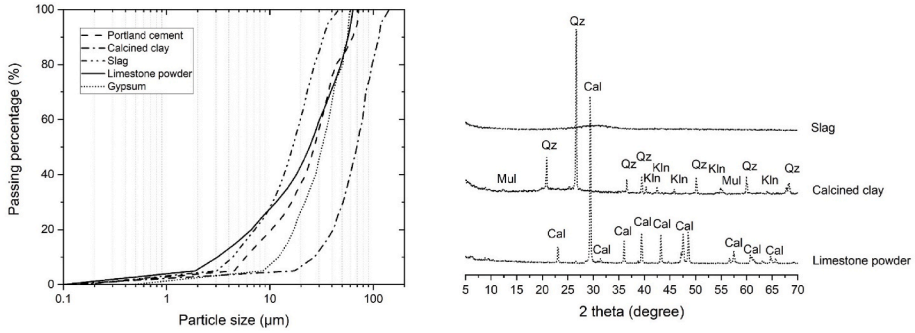

(a) (b)

Fig. 1. (a) Particle size distribution of calcined clay, slag, Portland cement, limestone powder, and gypsum; (b) X-ray diffraction (Cu-Kα radiation) patterns of calcined clay, slag, and limestone powder. Cal-calcite, Gp-gypsum, Mul-mullite, Qz-quartz, Kln-kaolinite.

Table 1
Oxide compositions of dry components determined by XRF analysis.

XRF [wt.%]	Calcined clay	Slag	Limestone powder	Portland cement
CaO	0.55	37.97	55.40	64.0
SiO_2	55.14	35.60	0.17	20.0
Al_2O_3	38.43	13.12	0.03	5.0
Fe_2O_3	2.60	0.37	0.04	3.0
K_2O	0.17	0.66	0	0
TiO_2	1.12	0	0	0
ZrO_2	0.05	0	0	0
SO_3	0	0.08	0	2.93
Other	1.94	12.20	44.36	5.07
Total	100.00	100.00	100.00	100.00

Table 2
Density and Brunauer-Emmett-Telle specific surface area of all binding materials.

	Calcined clay	Slag	Limestone powder	Portland cement	Gypsum
Density [g/cm^3]	2.51	2.95	2.65	3.17	2.32
SSA [m^2/g]	10.06	1.48	1.22	0.81	0.53

Table 3
Mix designs of the studied materials (wt% of the binder).

	Portland cement	Slag	LC2		Additional gypsum	Water
			Calcined clay	Limestone powder		
REF	100	0	0	0	0	40
A0	35	65	0	0	0	40
A30	35	35	20	10	0	40
A45	35	20	30	15	0	40
A45-1	35	18	30	15	2	40
A45-2	34	17.6	29.4	15	4	40
A65	35	0	43.4	21.6	0	40

can be beneficial to the hydration at a later age (28–90 days), resulting in an enhancement of mechanical performance at both early and later ages. They attributed the increased strength to the latent hydraulic reaction of slag as the portlandite consumption rate was promoted at a later stage. Furthermore, the addition of slag in LC3 can also modify the fresh properties of quaternary blended cement pastes. Compared to slag, calcined clay, with layered microstructure and extremely high specific surface area, shows much higher water and superplasticizer demands when used in cementitious materials, as reported by Refs. [15–18]. An earlier study [19] has attempted to mitigate this issue by incorporating fly ash in LC3. However, fresh-state properties of quaternary blended limestone-calcined clay cement incorporating slag have not been examined yet.

This study attempts to partially replace limestone and calcined clay with slag to improve the flow behavior and compressive strength of blended cement paste with a relatively low Portland cement content (about 35 wt%). The effect of decreasing limestone-calcined clay-to-slag ratio (LC2/slag) on fresh-state behaviors, i.e., fluidity, water retention capacity and rheology, of quaternary blended cement pastes was investigated. Furthermore, according to Refs. [10,20,21], due to the reactive aluminates in calcined clay and slag, additional gypsum should be added to quaternary blended cements to delay the aluminate reaction peak (sulfate depletion). The impact of gypsum addition on fresh properties was also studied. Additionally, the increase in slag content or gypsum dosage may influence the hydration kinetics and compressive strength of quaternary blended cement pastes. The heat released by hydration during the first 7 days and compressive strength at 3, 7, and 28 days of studied mixtures were measured. Finally, correlations between the obtained results and a discussion of the plausible mechanisms are given.

2. Material and methods

2.1. Materials

CEM I 42.5 N Portland cement, calcined clay, limestone powder, slag, and gypsum were used to produce the binding material in this study. Gypsum (>99% purity) was provided by Merck KGaA, Germany. Calcined clay containing about 50 wt% of metakaolin was purchased from Argeco, France. CEM I 42.5 Portland cement and Slag were supplied by ENCI Maastricht BV, the Netherlands, and Ecocem Benelux BV, the Netherlands, respectively. The particle size distribution of all fines measured by laser diffractometry (pure ethanol as the dispersant) is reported in Fig. 1 (a). Calcined clay displayed the coarsest particle size compared to other fines. Fig. 1 (b) presents X-ray diffraction (XRD) patterns (PhilipsPW1830 powder X-ray diffractometer with Cu-Kα radiation) of calcined clay, limestone powder and slag. It can be found that quartz was the main impurity of calcined clay. By using the chemical dissolution method [22], the content of reactive phases was about 48.8 wt% in calcined clay. Slag showed a very high amorphous content, and no crystalline phase was found in the XRD pattern. The chemical composition of Portland cement, calcined clay, limestone powder, and slag characterized using X-ray fluorescence (XRF) are summarized in Table 1. The calcium sulfate phases (gypsum and anhydrite) in Portland cement was about 5.7 wt%, which was determined using quantitative X-ray Diffraction analysis. Table 2 shows the density and Brunauer-Emmett-Telle (BET) specific surface area (SSA) of binding

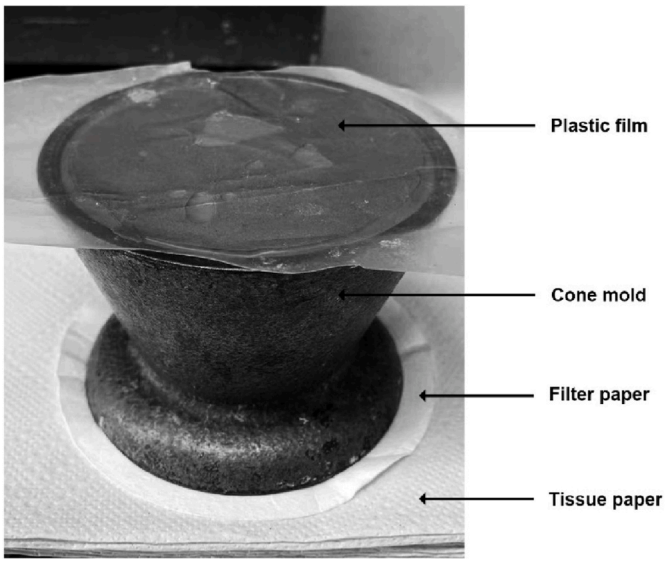

Fig. 2. Photograph of water retention test setup.

materials used. Calcined clay showed the coarsest grain size but the highest SSA compared to other fines. This is because the calcined clay used in this work is a blend of quartz and metakaolin. According to the observation from our earlier studies [13,23], metakaolin particles with thin layered, irregular flaky morphology adsorbed on the surface of quartz particles, resulting in large average grain size and very high SSA (see Appendix Figure A1). Note that the morphology of calcined clay could also influence the rheology of blended cementitious materials, as reported by Benkeser et al. [24].

All studied paste mixtures are presented in Table 3. The water-to-binder mass ratio of 0.4 was kept identical. Except for the REF mixture, all mixtures contained a similar Portland cement content (about 35 wt%). Compared to mixture A0, 46.2 wt% (30 wt% of the binder) and 69.2 wt% (45 wt% of the binder) of slag were replaced by the blend of calcined clay and limestone (LC2) in a mass ratio of 2:1. In mixture A65, the slag was entirely substituted by LC2. According to Ref. [20], additional gypsum may be required to avoid sulfate depletion in the very early-age hydration of calcined clay-based cementitious materials. After preliminary isothermal calorimetry screening, 2 wt% and 4 wt% of gypsum were added to the mixtures A45-1 and A45-2. Considering the pre-added calcium sulfate phases in Portland cement, the total calcium sulfate phases content in the binders of A45 (also A0 and A30), A45-1 and A45-2 were 2.0 wt%, 4.0 wt% and 5.9 wt%, respectively. Fresh paste samples (about 0.5 L) were prepared using a small planetary HOBART mixing machine and following the same protocol: after adding water, mix at low speed for 2 min and at high speed for 1.5 min. Time zero of fresh paste was defined as the time of adding water.

2.2. Test procedures

The fresh properties of studied mixtures, i.e., flow behaviors and structural build-up, were assessed using different approaches. Mini-slump flow, flow curve and strain sweep tests were conducted to determine the rheological characteristics of studied mixtures at material age of 10–22 min, including the spread diameter, dynamic yield stress, plastic viscosity, critical strain, and flow point. These characteristics can indicate the flowability of fresh mixtures, which is related to the pumping and transportation of fresh concrete. Structural build-up in relation to lateral pressure on the formwork of cast concrete and structuration rate of 3D printable concrete was evaluated using small amplitude oscillatory shear-time sweep (SAOS) test (material age: 22–82 min). Water retention capacity can indicate free water content, which is closely related to the rheology of studied mixtures. Moreover, isothermal calorimetry and compressive strength tests were applied to determine the influence of slag addition on hydration kinetics and strength development of the quaternary blended cement pastes.

2.2.1. Mini-slump flow and water retention tests

The mini-slump flow test was performed by using a metal cone mold with the dimensions of 40 mm in upper diameter, 75 mm in height, and 90 mm in bottom diameter. The mold was placed on a flat glass plate with a smooth surface. Before filling in the fresh paste, the inner surface of the cone mold was lubricated by mold oil. The fresh paste was filled in the mold 2–3 min after mixing. Afterward, the mold was slowly lifted at the material age of 10 min. The spread diameter of paste samples (when the paste stopped flowing) was recorded by measuring two perpendicular directions. The dimensionless spread diameter can be computed by using Eq (1).

$$D_s^{'} = D_s / D_{base} \tag{1}$$

$D_s^{'}$, D_s and D_{base} are the dimensionless spread diameter, measured spread diameter, and diameter of cone mold.

Water retention capacity is an indicator of free water content and is related to the rheology and flowability of fresh paste. In this study, the water retention test was based on the filter paper method proposed by Bülichen et al. [25]. As shown in Fig. 2, the cone mold (used in the mini-slump flow test) was inversed and placed on the top of paper stack, including a filter paper (glass microfiber filter, 1.6 μm sieve size, 100 mm diameter, Whatman™) and 15 folded tissue papers. Then, about 450 g of fresh paste at the material age of 10 min was carefully filled into the cone. A plastic film covered the sample's exposed surface to avoid water evaporation during testing. This test was performed at the material age from 22 min to 82 min. After 1 h, both the cone mold (with paste sample) and the filter paper were removed from the stacked tissue papers. The increase in weight of tissue papers was then recorded as the mass of absorbed water (W_{ab}). Note that the water absorbed by the filter paper was not included since the cementitious particles were also attached to the surface of the filter paper. Finally, the water retention can be calculated using Eq (2).

$$Water\ retention\ (\%) = \left(1 - \frac{W_{ab}}{W_0}\right) \times 100 \tag{2}$$

where W_0 is the weight of mixing water in the fresh paste.

2.2.2. Rheological tests

Flow curve and oscillatory shear tests were conducted to quantify the flow behavior and structural build-up of studied mixtures. An Anton Paar MCR 302e rheometer equipped with a cylindrical cup (28.92 mm inner diameter and 68 mm depth) and a four-blade vane (22 mm diameter and 40 mm height) was employed to conduct the rheological tests. The inner surface of the measuring cup had steel lamellas to reduce slippage. 85–90 g of fresh paste was filled into the measuring cup using a spoon for each measurement. The temperature of the measuring cup was kept at 20 °C using a Julabo refrigerated circulator. All rheological tests were conducted at least twice.

2.2.2.1. Flow curve test. The flow curve test protocol is illustrated in Fig. 3 (a). A pre-shear session (100 s^{-1} shear rate and 30 s duration) was executed at the material age of 8 min to ensure the same flow history of fresh samples. After 1.5 min of resting time (material age: 10 min), the shear rate ramped linearly from 0 s^{-1} to 100 s^{-1} within 1.5 min and was maintained at 100 s^{-1} for 45 s. After that, the shear rate was decreased in nine consecutive steps from 100 s^{-1} to 10 s^{-1} and was kept constant at about 45 s for each step. The data was recorded each 0.3 s. Fig. 3 (b) shows an example of shear stress vs. time curve using this test protocol. In the ascending regime, the shear stress developed rapidly within the first seconds after the test started. Afterward, the shear stress decreased

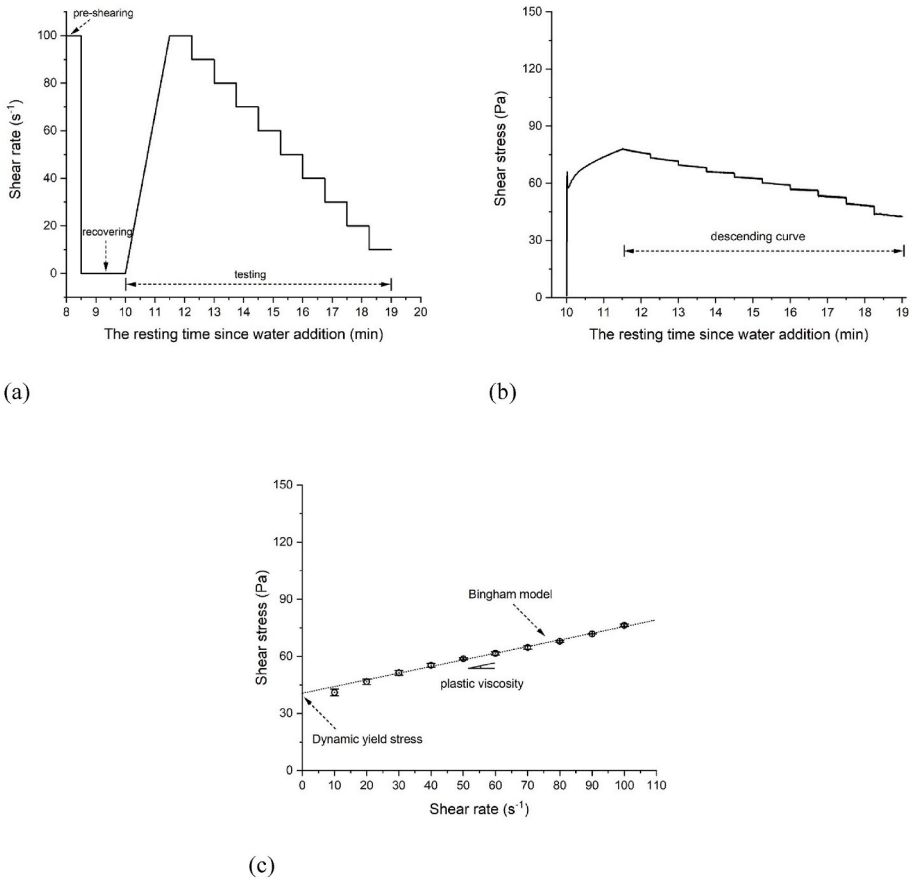

Fig. 3. (a) Protocol of flow curve test (b) A typical shear stress vs. testing time curve obtained using this test protocol; (c) The average shear stresses at the various shear rates from the descending curve were fitted by the Bingham model.

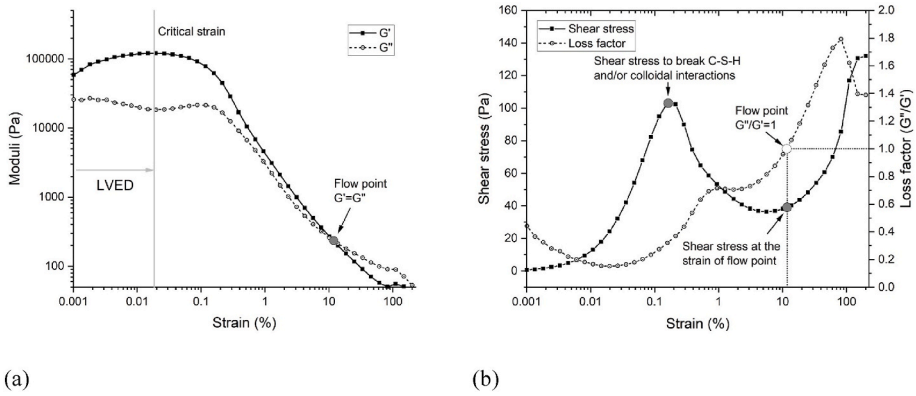

Fig. 4. Typical curves: (a) Moduli vs. applied strain obtained using strain sweep test; (b) Shear stress and loss factor vs. applied strain obtained using strain sweep test.

shortly and then increased with increasing the shear rate until reaching 100 s^{-1}. In the descending part, the shear stress displayed a slightly decreasing trend at the beginning and stabilized (exhibited a relative equilibrium value) after about 30 s for each shear rate step. Thus, the final 50 measuring points were averaged as the shear stress at the applied shear rate. In this study, the ascending part was employed to disrupt the flocculation of the cementitious particles, and the descending part was designed to characterize the flow behavior of studied pastes. The obtained shear stresses at the various shear rates from descending curve are plotted in Fig. 3 (c). The Bingham model was employed to determine the dynamic yield stress and the plastic viscosity of different mixtures.

$$\tau = \tau_d + \mu_p \dot{\gamma} \tag{3}$$

Here, τ is shear stress; τ_d and μ_p denote dynamic yield stress and plastic viscosity. $\dot{\gamma}$ is the applied shear rate.

2.2.2.2. Strain sweep and small amplitude oscillatory tests. According to Ref. [26], the theory of oscillatory shear test can be summarized as follows. A continuous sinusoidal oscillatory strain $\gamma(t)$ is applied to the fresh paste sample:

$$\gamma(t) = \gamma_0 \sin \omega t \tag{4}$$

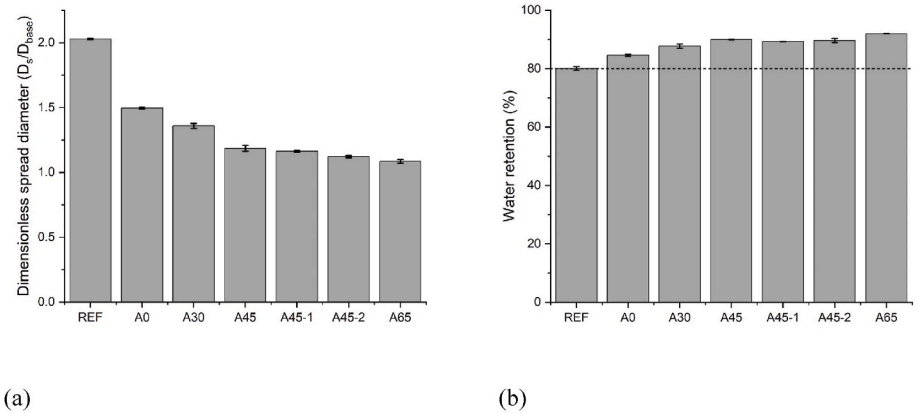

Fig. 5. (a) Mini-slump flow test results-dimensionless spread diameter of fresh mixture at 10 min; (b) Water retention test result (measured after 1 h). Error bars represent the standard deviation of repeated test results.

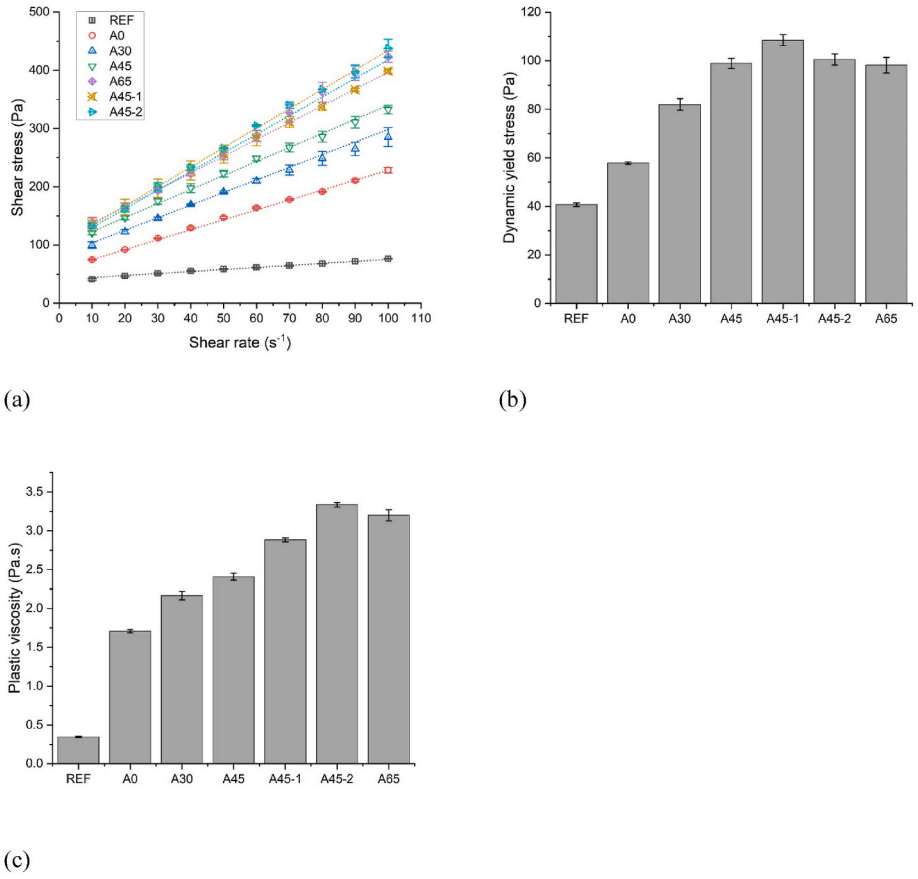

Fig. 6. (a) Flow curves – descending curves fitted by the Bingham model; (b) Dynamic yield stress of different mixtures; (c) Plastic viscosity of different mixtures. Error bars represent the standard deviation of repeated test results.

where γ_0 is the maximum strain amplitude. t and ω are time and frequency, respectively. The measured shear stress $\tau(t)$ can be presented as:

$$\tau(t) = G^*\gamma(t) \tag{5}$$

$$G^* = G' + iG'' \tag{6}$$

Here, G^* is the complex modulus. G' denotes the storage modulus representing the elastic component of stress. G'' means the loss modulus indicating the viscous component of stress. i is imaginary unit. In addition, the loss factor G''/G' (also known as $\tan(\delta)$. δ is the phase angle) was employed to describe the rigidity degree or liquid state of the tested material. The cementitious material shows a high rigidity when the G''/G' is approaching zero.

Prior to the test, the fresh sample at the material age of 7 min was pre-sheared with 100 s^{-1} for 30 s. After 30 s resting time, the strain sweep test with the applied strain of 0.001%–200% and a frequency of 1 Hz was executed. The test lasted about 14 min. Fig. 4 (a) shows the typical storage (G') and loss (G'') moduli vs. strain curves obtained using this method. Two indicators of the studied mixture, i.e., critical strain and flow point, can also be acquired. The critical strain in this context was defined as the maximum strain of the linear viscoelastic domain (LVED) [26,27]. According to Ref. [28], the flow point (occurring

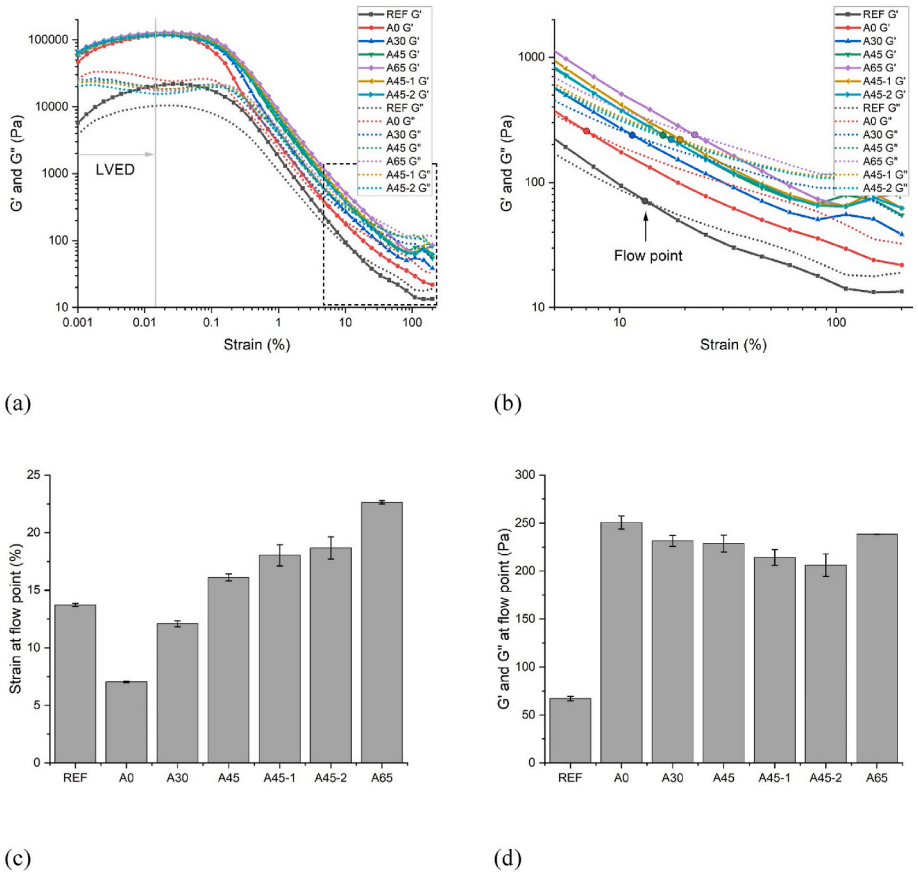

Fig. 7. Strain sweep test results: (a) G' and G'' moduli vs. applied strain (0.001%–200%); (b) G' and G'' moduli vs. applied strain (5%–200%); (c) Strain at the flow point for different mixtures; (d) G' and G'' moduli at the flow point for different mixtures. Error bars represent the standard deviation of repeated test results.

outside of LVED) can be defined as the crossover point of G' and G'' curves ($G' = G''$, or loss factor $G''/G' = 1$). After the flow point, the fresh paste displays more liquid-like behavior ($G' < G''$). As shown in Fig. 4 (b), shear stress (oscillation) vs. applied strain curve can also be determined in this test. The peak (about 0.1% applied strain) in the shear stress curve may be linked to the breakage of C–S–H links and/or colloidal interactions [29,30]. Note that the applied strain may be much larger than the effective strain because of "strain lag" [31]. In this study, shear stress to break C–S–H and/or colloidal interactions and shear stress at the flow point strain were also collected to compare the rheological behaviors of different mixtures.

SAOS test was used to monitor the structural build-up of fresh paste 10 s after the strain sweep test. G' is independent of the applied strain when the strain is smaller than the critical strain of LVED [32,33]. Based on the strain sweep test results (Section 3.3.), SAOS test was carried out at the maximum strain amplitude of 0.005%, which also agreed with the value in Refs. [27,34–36]. According to Refs. [26,37,38], 1 Hz of frequency, which is believed to be the suitable frequency for cementitious materials, was selected in this test. The test duration was about 1 h (material age: 22–82 min). The development of G' and G''/G' with time was employed to reveal the elasticity and rigidity of the formed network. The fresh mixture with high elasticity and structural build-up should show relatively high G' and low G''/G'.

2.2.3. Characterization of hydration kinetics and compressive strength

An eight-channel TAM Air isothermal calorimeter was employed to measure the hydration heat released in the first 7 days. In this test, 6 g of fresh paste was filled into a glass vessel (20 ml) after mixing the pre-weighed binding materials with the water by a small mixing machine for 3 min. The paste sample vessel and a reference vessel (filled with fine quartz sand) were placed in the isothermal calorimeter at 20 °C. The heat released by reactions was recorded every 55 s for 7 days.

Compressive strength of each mixture at 3, 7 and 28 days was measured using cast paste samples (40 mm cubic specimens). All samples were stored in sealed plastic bags at ambient temperature (about 20 °C). This curing condition ensured that no additional water was added to affect the hydration and strength development. For compressive strength testing, 2.4 kN/s of loading rate was used on the basis of NEN-EN 196–1 [39]. The reported compressive strength of each studied mixture at every age was the average value of three repeated tests.

3. Results

3.1. Mini-slump flow and water retention

Fig. 5 (a) shows the mini-slump flow value (dimensionless spread diameter) of various mixtures after removing the mold at the material age of 10 min. Compared to the plain cement paste (REF), all blended cement pastes exhibited a much lower spread diameter, indicating weaker flowability. The increase in LC2 content can further decrease this value. The spread diameter can also be slightly reduced by the addition of gypsum. This seems to contradict the results obtained by Ref. [40]. In the study by Akhlaghi et al. [40], the spread diameter is increased by increasing the dosage of gypsum. The addition of gypsum reduces the content of calcined clay, which may be the main cause for its enhanced flowability. However, the calcined clay content was kept (almost) identical, and only part of slag (and Portland cement in the case of mixture A45-2) was replaced by gypsum in this study. Please note that the differences between mixtures A45, A45-1 and A45-2 are statistically small if standard deviations are considered.

As shown in Fig. 5 (b), replacing 65 wt% Portland cement by slag and/or LC2 improved the water retention capacity of fresh paste. A high

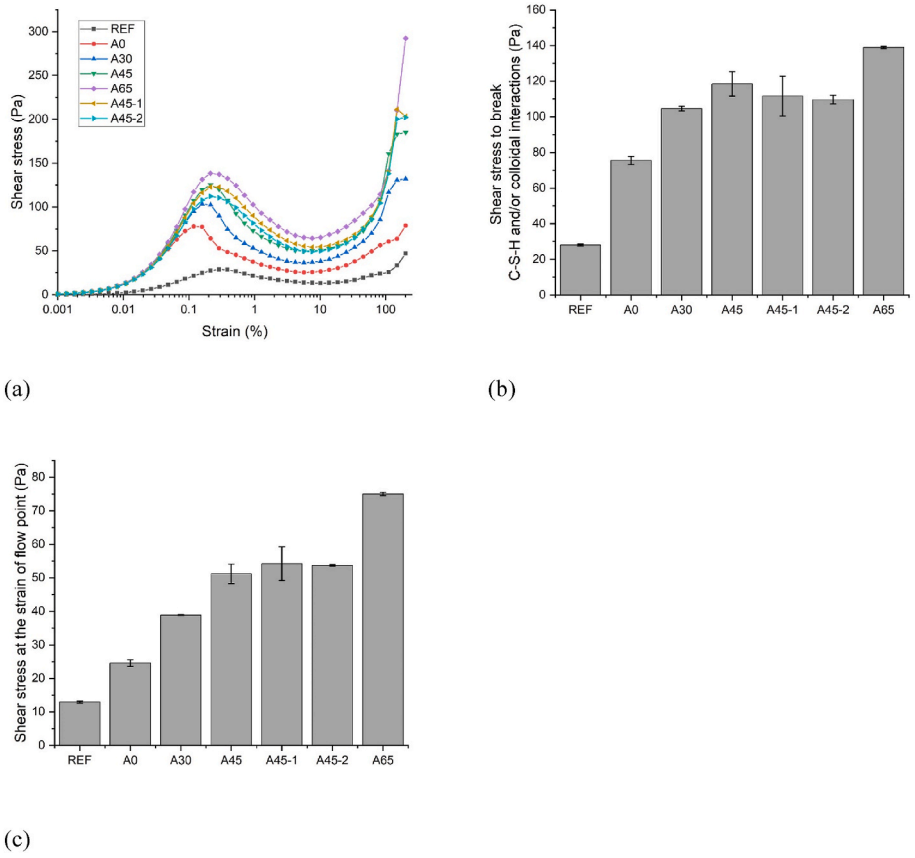

Fig. 8. Strain sweep test results: (a) Shear stress (oscillation) vs. applied strain; (b) The required shear stress to break C–S–H and/or colloidal interactions for different mixtures; (c) The shear stress at the strain of flow point for different mixtures. Error bars represent the standard deviation of repeated test results.

water retention property can be achieved by increasing the proportion of LC2. Mixture A65 displayed the highest water retention. The effect of gypsum on water retention was minor. In this context, the flowability reduction and enhancement of water retention may be related to the change in physical characteristics of the binder system induced by the LC2 substitution, which is further discussed in Section 4.2.

3.2. Flow curve

As shown in Fig. 6 (a), the mean shear stresses at the various shear rates from the descending curve were fitted by the Bingham model. The fitting results, including dynamic yield stress and plastic viscosity, were presented in Fig. 6 (b) (c). Both values generally increased by increasing LC2 content, except that the dynamic yield stress of mixture A65 was similar to that of mixture A45. The increase in the amount of gypsum significantly increased the plastic viscosity. The addition of 2 wt% gypsum still increased the dynamic yield stress compared to mixture A45, and the same value was maintained when adding 4 wt% gypsum. The increase in dynamic yield stress and plastic viscosity may be attributed to the presence of undissolved gypsum in the system. The dissolution of gypsum seems to be very slow within the first hour, according to the in-situ XRD results by Zunino and Scrivener [41]. Also, the increase of gypsum can increase the solid volume fraction, which may be responsible for the increase of dynamic yield stress and plastic viscosity. A different result was reported by Canbek et al. [42]. In their study, adding gypsum decreased LC3 proportion (especially the metakaolin content), which may be the main cause for the reduction of dynamic yield stress. In addition, the test protocol and materials are not the same compared with this study, which may also cause differences in test results.

3.3. Strain sweep and structural build-up

The storage modulus G' and the loss modulus G'' determined from the strain sweep measurement for different mixtures at 8 min are presented in Fig. 7 (a) (b). As can be observed, all G' curves displayed an increase in development with testing time within the LVED (the critical strain in the range of 0.01%–0.02% for all studied mixtures). As mentioned earlier, the measured G' is an independent value of the applied strain within LVED. Thus, the G' growth within LVED, similar to the SAOS test, was governed by the flocculation and nucleation of cementitious particles at rest [43]. After the critical strain, G' started to decrease with increasing shear strain, which was due to the destruction of the flocculated microstructure. For all blended cement pastes, a small hump appeared in the G'' curve within LVED, and a small shoulder was found before the large deformation of microstructure (0.1%–0.2% applied strain). The small hump in G'' curve within LVED may be related to the gelation process of cementitious materials, as explained in Refs. [34,44]. The small shoulder (which appeared at 0.1%–0.2% applied strain) indicated the increase in dissipated energy, which may be attributed to the relative motion between flocculated/agglomerated particles [28]. G' and G'' decreased almost linearly over the applied strain range of 0.2%–50%. The crossover point of G' and G'' curves ($G' = G''$), denoted as flow point, was also found in this strain range. The applied strain, as well as G' and G'' moduli at the flow point, were collected and plotted in Fig. 7 (c) (d). For blended cement pastes, the increase in LC2 content can significantly increase the required strain of flow point. Also, mixtures with additional gypsum (A45-1 and A45-2) showed a higher strain than mixture A45. However, G' and G'' moduli at the flow point were quite similar for these blended cement pastes, and were much larger than that of mixture REF.

Fig. 8 (a) illustrates the shear stress (oscillation) response to the applied shear strain in the strain sweep test. Blended cement pastes

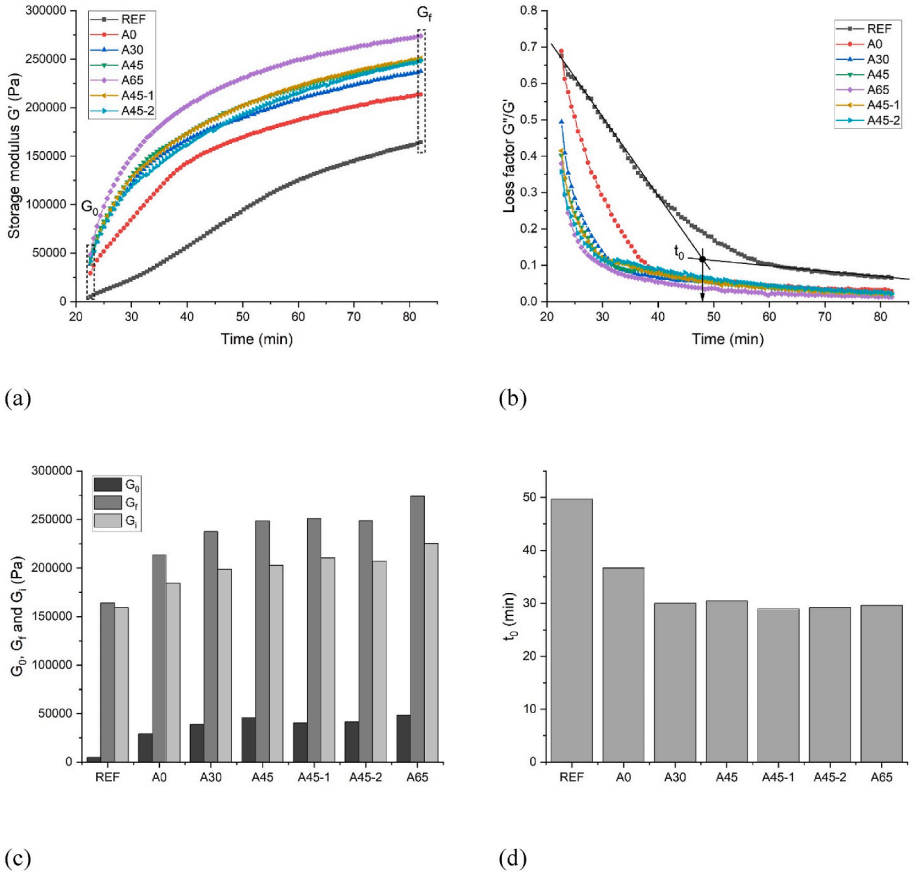

Fig. 9. Small amplitude oscillatory test result: (a) Storage modulus with time; (b) Loss factor with time; (c) Initial storage modulus G_0, final storage modulus G_f, and increment of storage modulus $G_i = G_f$-G_0; (d) Percolation time t_0 of different mixtures.

needed much higher shear stress to break C–S–H links and/or colloidal interactions (Fig. 8 (b)) and the corresponding shear strain was smaller than the REF mixture. Increasing the substitution of LC2 for slag can increase the shear stress and the shear strain required for the peak. The increase in gypsum amount did not modify the required shear strain, but it decreased the shear stress to break C–S–H links and/or colloidal interactions. Additionally, based on the flow point strain in Fig. 7 (c), the shear stress at the flow point for different mixtures was collected in Fig. 8 (c). This value was also increased by increasing LC2 content. The addition of 2–4 wt% gypsum showed negligible influence on the shear stress compared to mixture A45.

Fig. 9 (a) (b) show the SAOS test results, i.e., development of storage modulus (G'), and loss factor (G''/G') from the resting time of 22 min–82 min. For most of mixtures, G' and G''/G' developed rapidly within the first 10 min (about 15 min and 30 min for mixtures A0 and REF) of the testing time. This may be attributed to forming a network of colloidal interactions induced by the flocculation of cementitious particles [30,45,46]. After that, the increase in G' became slower, and G''/G' approached zero, which may be linked to the precipitation of C–S–H at the pseudo-contact points between flocculated particles, resulting in the formation of a percolated rigid network [47,48]. The initial and final values (G_0 and G_f) extracted from G' curves, as well as the increment during the testing time (G_i), were compared in Fig. 9 (c). It can be found that the increase in LC2 content boosted the elasticity development (G_i) of fresh paste within the first 1.5 h. The addition of gypsum slightly reduced the initial storage modulus (G_0), but did not affect the elasticity growth (G_i) during the testing time. The transition time between two stages in Fig. 9 (b) was defined as the percolation time (t_0), according to Refs. [46,49]. As shown in Fig. 9 (d), compared to the REF mixture, all blended cement pastes needed less time to form percolated network. Mixtures with LC2 displayed a similar t_0, shorter than the slag-cement paste (A0).

3.4. Isothermal calorimetry

Fig. 10 shows the isothermal calorimetry test results of all blended cement pastes. The heat flow within the first 56 h, normalized by paste mass, is presented in Fig. 10 (a). After the initial heat release induced by the particle wetting and C_3A dissolution [50], a small peak was found in mixtures containing LC2 in the first hour of hydration, as shown in Fig. 10 (b). This may be related to the temporary gypsum depletion caused by the slow dissolution of gypsum within the first 1 h [10,41,51] and/or sulfate adsorption on C-(A)-S-H surfaces or calcined clay (metakaolin) particle surfaces [10,41]. As can be observed, the intensity of this peak increased with the increasing proportion of LC2. For mixtures A45, A45-1, and A45-2, the intensity of this peak was almost not modified by increasing the gypsum content. After that, the intensity of all curves decreased during the dormant period. Increasing LC2 content increased the intensity of the bottom point but delayed the onset of the acceleration stage. The increased intensity of the bottom point can be attributed to the increase in Al_2O_3 content caused by the increase in calcined clay content. Fig. 10 (f) shows a good linear correlation between the heat flow value at the bottom point and Al_2O_3 content in the blended mixture. Nevertheless, the mechanism associated with this enhancement remains unrevealed and deserves further exploration. After the acceleration stage, the C_3S peak of mixtures A45-1, and A45-2 appeared at the very similar time (around 9 h of hydration). For mixtures A30, A45 and A65, the main hydration peak overlapped with aluminate peak [10,52], resulting in a sharp, narrow, and high intensity peak. The aluminate peak of mixture A0 appeared after the C_3S peak.

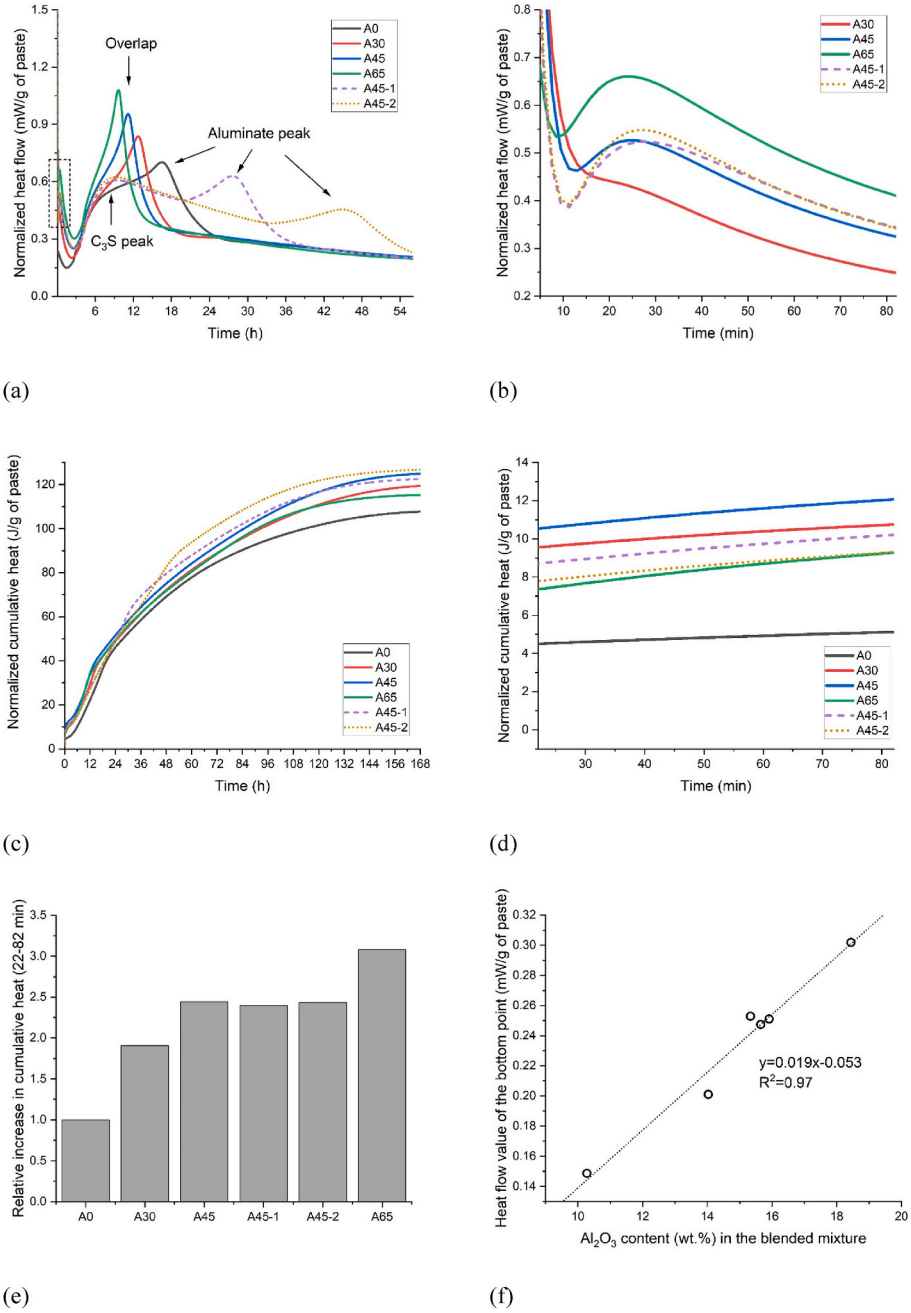

Fig. 10. Isothermal calorimetry test results: (a) Normalized heat flow by paste mass with time (56 h); (b) Normalized heat flow by paste mass with time (5–82 min). The displayed area is within the dashed frame of Fig. 10 (a); (c) Normalized cumulative heat by paste mass with time (168 h); (d) Normalized cumulative heat by paste mass with time (22–82 min); (e) The increase in normalized cumulative heat relative to the rise in mixture A0 (22–82 min); (f) The linear relationship between heat flow value at the bottom point and Al_2O_3 content in the blended mixture.

Additionally, increasing the gypsum content in mixture A45 significantly delayed the appearance time and intensity of the aluminate peak.

The cumulative heat of different mixtures normalized by paste weight over the first 7 days is reported in Fig. 10 (c). Mixture A0 exhibited the lowest heat value during testing compared to others. Increasing LC2 content from 30 wt% to 45 wt% can increase the cumulative heat, whereas replacing all slag with LC2 resulted in a lower value than mixture A30 at 7 days. Mixtures with additional 2 wt% and 4 wt% gypsum (A45-1 and A45-2) showed a higher cumulative heat than mixture A45 from 27 h to 34 h, respectively. Finally, all three mixtures displayed a similar value at 7 days. Fig. 10 (d) illustrates the normalized cumulative heat for different studied mixtures from 22 min to 82 min (the same time range as the SAOS test). All curves displayed an almost linear increase over time. The increase in cumulative heat relative to the rise in mixture A0 is presented in Fig. 10 (e). It can be found that the relative growth of cumulative heat was enhanced by increasing the proportion of LC2. Mixtures with different gypsum contents exhibited similar values.

3.5. Compressive strength

Fig. 11 shows compressive strength of different paste samples at 3, 7 and 28 days. Compared to mixture A0, mixtures with LC2 and slag (A30 and A45) displayed slightly higher compressive strength at 3 days. The addition of gypsum (A45-1 and A45-2) further enhanced the 3-day compressive strength to more than 20 MPa. This enhancement can be attributed to delayed sulfate depletion [20]. As mentioned in Refs. [51, 53], C_3S hydration degree and early-age strength can be severely reduced if the aluminate reaction peak occurs before and/or during the C_3S hydration peak caused by insufficient sulfate addition. As shown in Fig. 10 (a), the aluminate peaks in mixtures A45-1 and A45-2 were significantly delayed compared to mixture A45. Mixture A0 showed

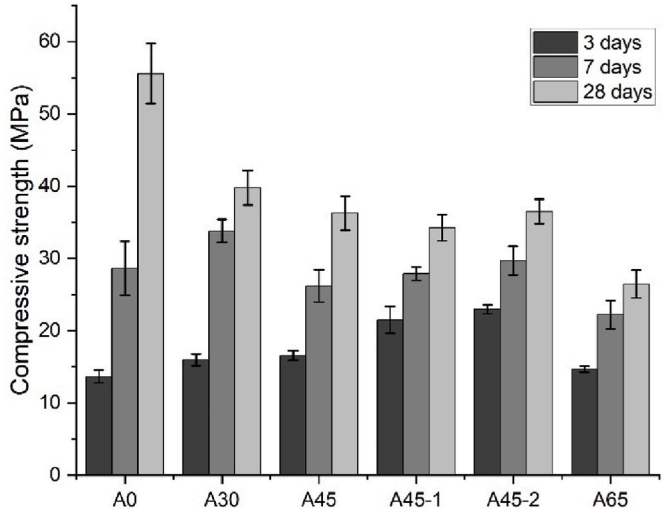

Fig. 11. Compressive strength of paste samples at 3, 7 and 28 days. Error bars represent the standard deviation of repeated test results.

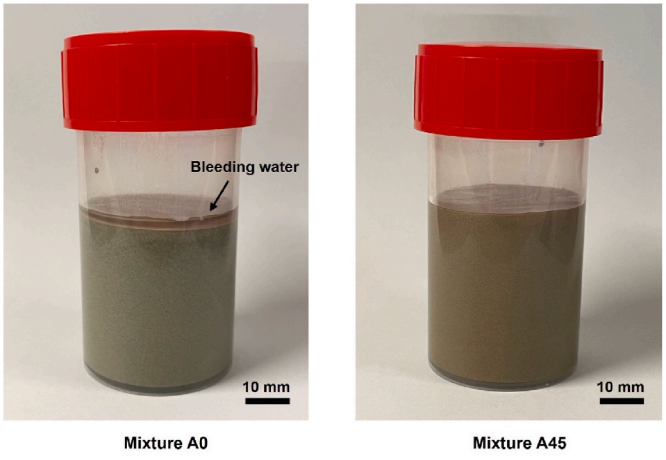

Fig. 12. Bleeding observation: (Left) Mixture A0 at 120 min of resting time; (Right) Mixture A45 at 120 min of resting time.

similar compressive strength compared with mixtures A45, A45-1 and A45-2, but slightly lower than mixture A30 at 7 days. The compressive strength development from 7 days to 28 days of mixtures with LC2 and slag (A30 and A45) was much smaller than mixture A0. Increasing LC2 content decreased the 28-day compressive strength. Also, adding gypsum did not improve the compressive strength at 28 days. Mixture A65 containing 0 wt% of slag exhibited slightly higher compressive strength than mixture A0 at 3 days, but had the lowest strength at 7 and 28 days.

The latent hydraulic properties of slag may be the leading cause for the enhancement of 28 days compressive strength in this context [54]. Such an effect was activated by the high pH (>13) in the pore solution [55]. Replacing slag with calcined clay diluted the impact of slag. Also, according to Refs. [20,23,56], calcined clay consumed CH within the first 7 days due to the pozzolanic reaction, which can lower the pH of pore solution and thus adversely affect the latent hydraulic reactions of slag. Additionally, a large amount of bleeding water was observed in mixture A0 after 120 min of resting time, which was much higher than in mixtures with calcined clay (see Fig. 12). This can also be confirmed by the water retention test results (see Fig. 5 (b)). Most of the bleeding water evaporated during air curing (20–25 °C, 40–45% RH), resulting in the decrease in the actual water-to-binder mass ratio in mixture A0, which may also be one of the reasons for its high compressive strength at 28 days.

4. Discussion

4.1. Correlation between mini-slump flow and rheological characteristics

According to earlier studies [57,58], the mini-slump flow test results can be employed to predict yield stress. Li et al. [59] proposed generalized models (see Eqs (7–10)) to precisely predict the yield stress using the spread diameter of fresh pastes based on empirical models by Refs. [57,60]:

$$\tau_y' = \tau_y \Big/ \rho g H_{eq} = \frac{1}{\beta} exp\left(-aD_s' - b\right) \tag{7}$$

$$H_{eq} = H_{cone}/\beta \tag{8}$$

$$\beta = 3(1+\lambda)^2 \Big/ \left(3\lambda^2 + 3\lambda + 1\right) \tag{9}$$

$$\lambda = R_{top} \Big/ \left(R_{base} - R_{top}\right) \tag{10}$$

where τ_y' and τ_y stand for dimensionless dynamic yield and measured dynamic yield stress in Section 3.2. ρ is the density of paste (kg/m^3); g is the gravitational acceleration (m/s^2); H_{eq} is the cone equivalent to cylinder height; H_{cone} is the cone height; β is the corrective coefficient; λ is the geometric parameter of the cone. R_{top} and R_{base} are the top and bottom radii of cone mold; a and b denote fitting parameters. By using this model, a strong correlation between the dimensionless dynamic yield stress and dimensionless spread diameter can be determined (R^2 >

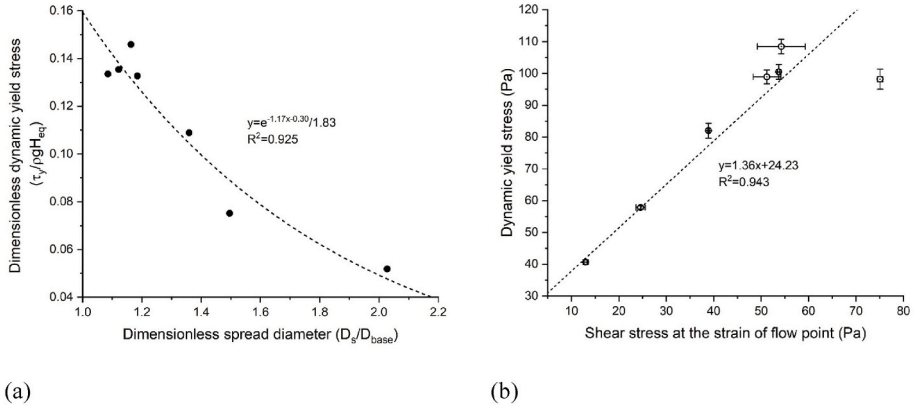

Fig. 13. Correlation between: (a) Dimensionless dynamic yield stress and dimensionless spread diameter; (b) Dynamic yield stress (flow curve test) and shear stress at the strain of flow point (strain sweep test).

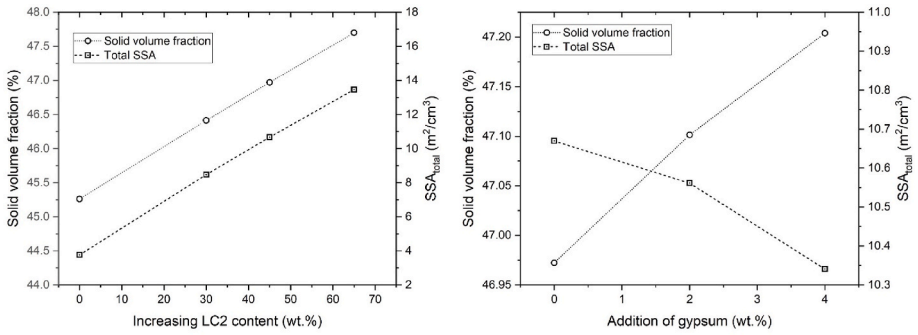

Fig. 14. (a) Influence of increasing LC2 content on solid volume fraction and total specific surface area of the binder; (b) Influence of increasing gypsum content on solid volume fraction and total specific surface area of the binder.

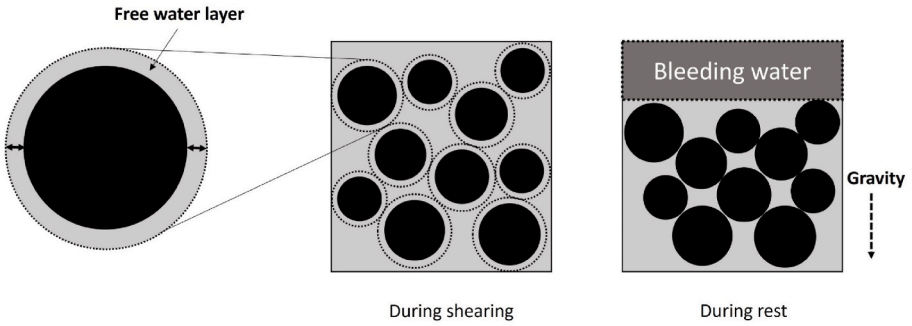

Fig. 15. Illustration of free water layer that can lubricate the cementitious particles during shearing and becomes bleeding water during the resting time.

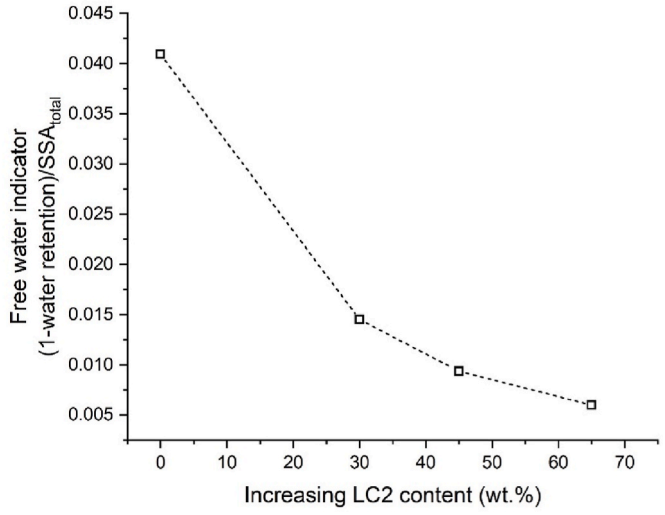

Fig. 16. Effect of increasing LC2 content on free water indicator.

0.9), as shown in Fig. 13 (a).

Fig. 13 (b) demonstrates a highly positive linear relationship between dynamic yield stress (flow curve test) and shear stress at the flow point strain (strain sweep test). According to Qian et al. [61], dynamic yield stress is defined as the minimum force needed to maintain or stop the flow of a fresh mixture. As mentioned in Section 3.3, the flow point ($G' = G''$) coincided with a transition boundary between more liquid-like ($G'<G''$) and more solid-like ($G'>G''$) behavior of fresh pastes. Thus, both values showed strong similarities and correlations.

4.2. Effect of increasing LC2 content on fresh properties

Replacing slag with LC2 changed not only the chemical composition, but also the physical characteristics of the binder, which appeared to play a dominant role in the modification in fresh properties. As shown in Fig. 14 (a), the solid volume fraction (φ) and the total specific surface area (SSA_{total}) of the binder increased with increasing the proportion of LC2. The solid volume fraction increased by about 2.5% by increasing the content of LC2 from 0 to 65 wt%. In contrast, SSA_{total} displayed a more significant increase induced by the extremely high SSA of calcined clay. The addition of gypsum could also slightly modify these physical characteristics, although such changes were very limited (Fig. 14 (b)). The increase in solid volume fraction and SSA_{total} could be the main cause for the enhancement of water retention capacity. The former reduced the total water volume, and the latter increased the water absorption [62].

As mentioned in Section 4.1, the free water content can be revealed by the water retention capacity of fresh pastes. The free water in the fresh paste mainly played a lubricating role during shearing, and became the bleeding water during the resting time (Fig. 15). It can be assumed that the surface of cementitious particles was covered by free water, which mitigated the interactions (i.e., colloidal attractive forces and frictions) between flocculated particles. In this context, a free water indicator (similar to free water film thickness [63]) is proposed as follows:

$$Free\ water\ indicator = (1 - water\ retention) \,/\, SSA_{total} \tag{11}$$

As shown in Fig. 16, the free water indicator decreased with increasing LC2 contents.

Fig. 17 (a) shows that the increase in LC2 resulted in the relative increase in cumulative heat and G' during material age of 22–82 min (both are relative to the value of mixture A0). As mentioned earlier, the growth of G' is related to the attractive colloidal interactions at the

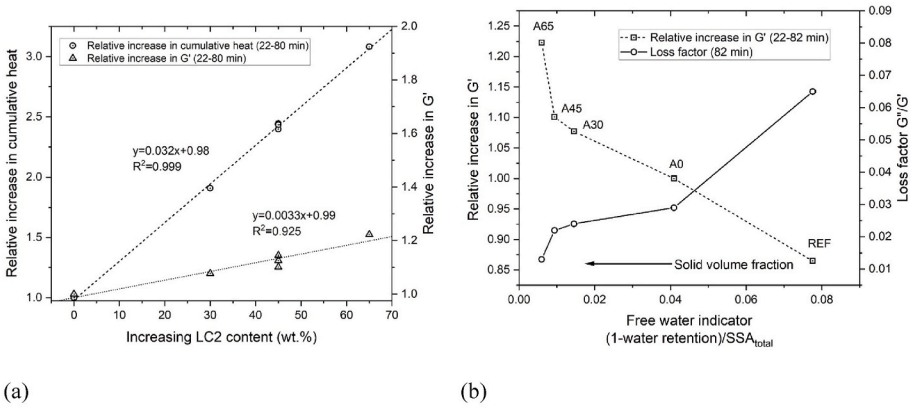

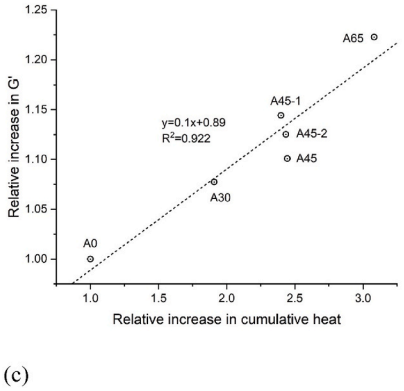

Fig. 17. (a) The effect of increasing LC2 content on the increase in relative cumulative heat and relative increase in storage modulus G' during material age of 22–82 min (both are relative to the value of mixture A0); (b) Correlation between free water indicator and relative increase in storage modulus G' during material age of 22–82 min (relative to the value of mixture A0) or loss factor at 82 min; (c) Correlation between the relative increase in cumulative heat and storage modulus G' during material age of 22–82 min (both are relative to the value of mixture A0).

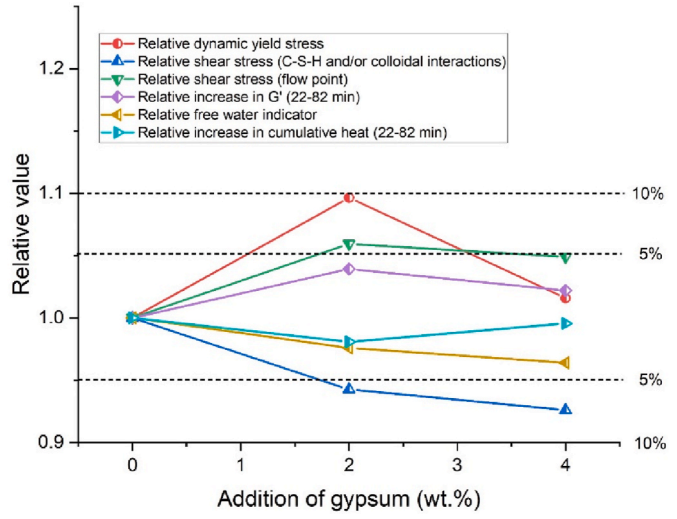

Fig. 18. Influence of increasing gypsum content on rheological characteristics, evolution of elasticity and rigidity (22–82 min), free water indicator and early-age hydration (22–82 min). All plotted values were relative to the value of mixture A45 (0 wt% gypsum). The dashed lines represent the relative change of 5% and 10%.

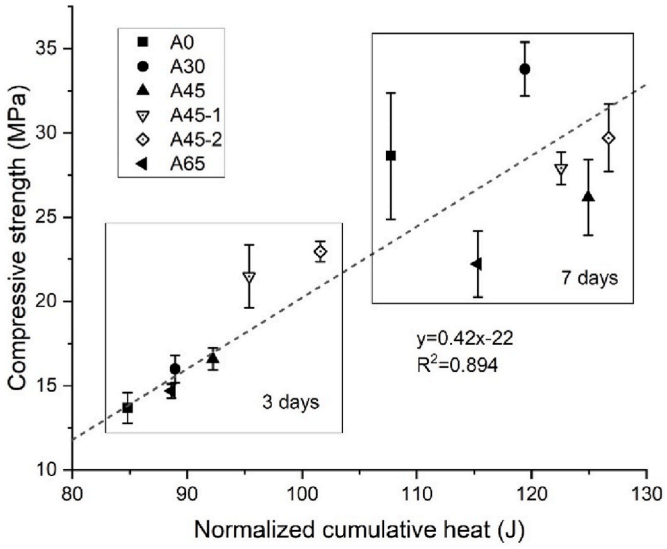

Fig. 19. A linear correlation between 3- and 7-day compressive strength and normalized cumulative heat by mass of paste.

beginning and C–S–H bridge between particles after the percolation time [64]. Cementitious material systems with high particle concentration (solid volume fraction), and short interparticle distance typically need a short characteristic flocculation time to form a percolation path [30]. As shown in Fig. 17 (b), increasing LC2 content increased the solid volume fraction and decreased the free water indicator, contributing to the growth of elasticity and rigidity of fresh paste (the increase in G' and decrease in loss factor). The decrease in the free water indicator may increase the shear force between particles and promote the nucleation and growth of hydrates [65].

The rise in cumulative heat (22–82 min) may be ascribed to the acceleration of C_3A dissolution induced by the temporary gypsum depletion (see Fig. 10 (b)) due to the addition of calcined clay. According to Gauffinet-Garrault [48], the hydration products of C_3A can support the development of C–S–H, contributing to the increase in G'. However, the mechanical efficiency of C–S–H (the ratio of increase in G' to cumulative

heat gain) can only be improved when C_3A is added in large quantities (>20%). Although a linear correlation can be established between the relative increase in cumulative heat and *G'* (22–82 min) in Fig. 17 (c), further studies are needed to reveal the mechanism. In addition, increasing the content of LC2 increases Al_2O_3 content in the blended mixture, as shown in Fig. 10 (f). Similar to the increase in SSA, the increase in Al_2O_3 content is also caused by the increased content of calcined clay (metakaolin) in the mixture, because calcined clay (metakaolin) is composed of a layered structure consisting of Si-centered tetrahedral sheets alternating with Al-centered octahedral sheets [66]. The increase of Al_2O_3 content may be one of the reasons for the rise in cumulative heat and *G'* during material age of 22–82 min. However, the role of Al_2O_3 from calcined clay (metakaolin) in the structural build-up and early-age hydration of cementitious materials still needs to be investigated in future work.

4.3. Effect of increasing gypsum dosages on fresh properties and compressive strength

Fig. 18 compares the influence of increasing gypsum content on the dynamic yield stress, shear stress (to break C–S–H and/or colloidal interactions and at the strain of flow point), growth of *G'* (22–82 min), free water indicator, and increase in cumulative heat (22–82 min). Most features were barely modified by adding gypsum (within 5% relative change).

Fig. 19 presents a linear correlation between compressive strength (3 and 7 days) and normalized cumulative heat. At 3 days, the mixtures with a high compressive strength also showed a high cumulative heat value. The addition of gypsum delayed/extended the aluminate reaction and could mitigate the inhibition of aluminate ions on C_3S dissolution and hydration [12,67,68], resulting in a considerable increase in the released heat of hydration. The improvement of compressive strength may be attributed to the enhancement of C–S–H formation induced by the high sulfate concentration in the pore solution during the main alite reaction period [69]. After that, mixtures with high compressive strength did not always show high cumulative heat. This is because the pozzolanic reaction induced by calcined clay and/or latent hydraulic reaction caused by slag generated much lower heat than alite hydration [3,23,56]. In the current work, the addition of gypsum to the quaternary blended pastes improved the compressive strength at 3 days, but did not modify the compressive strength at 7 and 28 days. Gypsum appears to play a more dominant role at the early age of cement hydration.

5. Conclusions

This study attempted to develop quaternary blended cements containing Portland cement, slag, limestone, and calcined clay. The effects of two material parameters, i.e., limestone-calcined clay-to-slag ratio (LC2/slag), and gypsum content, on fresh properties, hydration kinetics, and compressive strength have been systematically investigated. The main findings of the current study were summarized as follows.

- The decrease in LC2 content increased the flowability and decreased the water retention capacity, rheological characteristics (including dynamic yield stress, plastic viscosity, strain at the flow point, the shear stress required to break C–S–H and/or colloidal interactions and to reach the flow point), and structural build-up (i.e., the growth of *G'* over 22–82 min). The addition of gypsum barely modified most of the fresh properties.
- The modification of fresh properties induced by the increase in LC2 content appears to be related to the low free water content (high water retention capacity), which may be governed by the strong water absorption of calcined clay particles. Therefore, a free water indicator (the ratio between free water content and SSA_{total} of the binder) was proposed, and is strongly correlated to the growth of structural build-up metrics.
- Mini-slump flow test is simple and efficient method to quantify the flow behaviors of fresh pastes. Good correlations ($R^2 > 0.9$) between mini-slump flow and rheological characteristics obtained using rheometry (dynamic yield stress from flow curve test) were determined.
- The time and the intensity of the aluminate peak due to gypsum depletion was shortened and enhanced with increasing LC2 content, leading to an overlap with the C_3S hydration peak. The increase in cumulative heat over 22–82 min was augmented by increasing LC2 content, which appeared to be related to the increase in *G'*.
- The addition of gypsum can delay the time of the aluminate peak and significantly improve compressive strength at 3 days but has limited effect on 7- and 28-day compressive strength. The mixture with higher slag content displayed higher compressive strength at 28 days, which can be attributed to the latent hydraulic reaction of slag and the decrease in water-to-binder mass ratio caused by the severe bleeding.

With the results obtained in this study, it can be found that the fresh properties, hydration, and compressive strength were significantly influenced by the LC2/slag ratio (0.9–2.5) and the additional gypsum (2–4 wt% of the binder). The proportion of LC2 in the quaternary blended cements can be adjusted in accordance with the specific requirements of the application. For example, increasing LC2 content may be beneficial for implementing the quaternary blended cements in 3D concrete printing or alleviating bleeding in cast concrete. In contrast, improving flowability and compressive strength from 28 days can be achieved by increasing the slag proportion. Adding gypsum is very useful if the high early-age compressive strength (e.g., 3 days) is required.

Declaration of competing interest

The authors declare that they have no known competing financial interests or personal relationships that could have appeared to influence the work reported in this paper.

Data availability

Data will be made available on request.

Acknowledgments

Yu Zhang would like to acknowledge the funding supported by China Scholarship Council under grant No. 201808320456. Dr. Branko Šavija acknowledges the financial support of the European Research Council (ERC) within the framework of the ERC Starting Grant Project “Auxetic Cementitious Composites by 3D printing (ACC-3D)”, Grant Agreement Number 101041342.

Appendix

Figure A1 shows the morphology of calcined clay particles under secondary electron (SE) mode of scanning electron microscopy (SEM). It can be found that the metakaolin particles with thin layered, irregular flaky morphology are adsorbed on the surface of quartz particles.

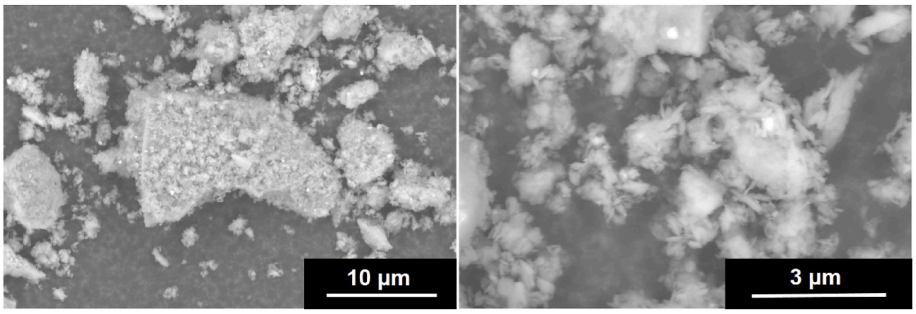

Fig. A1. Electron micrograph of calcined clay. (Left) 10000*x* magnification; (Right) 40000*x* magnification. Adapted from Ref. [23].

References

[[1] M.C.G. Juenger, F. Winnefeld, J.L. Provis, J.H. Ideker, Advances in alternative cementitious binders, Cement Concr. Res. 41 (2011) 1232–1243, https://doi.org/10.1016/j.cemconres.2010.11.012.

[2] B. Lothenbach, K. Scrivener, R.D. Hooton, Supplementary cementitious materials, Cement Concr. Res. 41 (2011) 1244–1256, https://doi.org/10.1016/j.cemconres.2010.12.001.

[3] Z. Giergiczny, Fly ash and slag, Cement Concr. Res. 124 (2019), 105826, https://doi.org/10.1016/j.cemconres.2019.105826.

[4] Y. Zhang, S. Zhang, Y. Chen, O. Çopuroğlu, The effect of slag chemistry on the reactivity of synthetic and commercial slags, Construct. Build. Mater. 335 (2022), 127493, https://doi.org/10.1016/j.conbuildmat.2022.127493.

[5] EN 197-1, Cement - Part 1: Composition, Specifications and Conformity Criteria for Common Cements, NEN, 2000, pp. 178–184, https://doi.org/10.1016/0005-2736(80)90400-9.

[6] K. Scrivener, F. Martirena, S. Bishnoi, S. Maity, Calcined clay limestone cements (LC3), Cement Concr. Res. 114 (2018) 49–56, https://doi.org/10.1016/j.cemconres.2017.08.017.

[7] R. Snellings, Assessing, understanding and unlocking supplementary cementitious materials, RILEM Tech. Lett. 1 (2016) 50, https://doi.org/10.21809/rilemtechlett.2016.12.

[8] F. Zunino, K. Scrivener, Microstructural developments of limestone calcined clay cement (LC3) pastes after long-term (3 years) hydration, Cement Concr. Res. 153 (2022), 106693, https://doi.org/10.1016/j.cemconres.2021.106693.

[9] M. Sharma, S. Bishnoi, F. Martirena, K. Scrivener, Limestone calcined clay cement and concrete: a state-of-the-art review, Cement Concr. Res. 149 (2021), 106564, https://doi.org/10.1016/j.cemconres.2021.106564.

[10] F. Zunino, K. Scrivener, The influence of the filler effect on the sulfate requirement of blended cements, Cement Concr. Res. 126 (2019), 105918, https://doi.org/10.1016/j.cemconres.2019.105918.

[11] T. Matschei, B. Lothenbach, F.P. Glasser, The role of calcium carbonate in cement hydration, Cement Concr. Res. 37 (2007) 551–558, https://doi.org/10.1016/j.cemconres.2006.10.013.

[12] J. Skibsted, R. Snellings, Reactivity of supplementary cementitious materials (SCMs) in cement blends, Cement Concr. Res. 124 (2019), 105799, https://doi.org/10.1016/j.cemconres.2019.105799.

[13] Y. Chen, S. He, Y. Zhang, Z. Wan, O. Çopuroğlu, E. Schlangen, 3D printing of calcined clay-limestone-based cementitious materials, Cement Concr. Res. 149 (2021), 106553, https://doi.org/10.1016/j.cemconres.2021.106553.

[14] H. Wang, P. Hou, Q. Li, S. Adu-Amankwah, H. Chen, N. Xie, P. Zhao, Y. Huang, S. Wang, X. Cheng, Synergistic effects of supplementary cementitious materials in limestone and calcined clay-replaced slag cement, Construct. Build. Mater. 282 (2021), 122648, https://doi.org/10.1016/j.conbuildmat.2021.122648.

[15] H. Paiva, A. Velosa, P. Cachim, V.M. Ferreira, Effect of metakaolin dispersion on the fresh and hardened state properties of concrete, Cement Concr. Res. 42 (2012) 607–612, https://doi.org/10.1016/j.cemconres.2012.01.005.

[16] N. Nair, K. Mohammed Haneefa, M. Santhanam, R. Gettu, A study on fresh properties of limestone calcined clay blended cementitious systems, Construct. Build. Mater. 254 (2020), 119326, https://doi.org/10.1016/j.conbuildmat.2020.119326.

[17] Y. Chen, S. He, Y. Gan, O. Çopuroğlu, F. Veer, E. Schlangen, A review of printing strategies, sustainable cementitious materials and characterization methods in the context of extrusion-based 3D concrete printing, J. Build. Eng. 45 (2022), 103599, https://doi.org/10.1016/j.jobe.2021.103599.

[18] S. Bhattacherjee, A.S. Basavaraj, A.V. Rahul, M. Santhanam, R. Gettu, B. Panda, E. Schlangen, Y. Chen, O. Copuroglu, G. Ma, L. Wang, M.A. Basit Beigh, V. Mechtcherine, Sustainable materials for 3D concrete printing, Cem. Concr. Compos. 122 (2021), 104156, https://doi.org/10.1016/j.cemconcomp.2021.104156.

[19] A. Dixit, H. Du, J. Dang, S.D. Pang, Quaternary blended limestone-calcined clay cement concrete incorporating fly ash, Cem. Concr. Compos. 123 (2021), 104174, https://doi.org/10.1016/j.cemconcomp.2021.104174.

[20] M. Antoni, J. Rossen, F. Martirena, K. Scrivener, Cement substitution by a combination of metakaolin and limestone, Cement Concr. Res. 42 (2012) 1579–1589, https://doi.org/10.1016/j.cemconres.2012.09.006.

[21] F. Avet, E. Boehm-Courjault, K. Scrivener, Investigation of C-A-S-H composition, morphology and density in limestone calcined clay cement (LC3), Cement Concr. Res. 115 (2019) 70–79, https://doi.org/10.1016/j.cemconres.2018.10.011.

[22] NEN-EN 196-2, Method of Testing Cement - Part 2: Chemical Analysis of Cement, 2013.

[23] Y. Chen, C.R. Rodriguez, Z. Li, B. Chen, O. Çopuroğlu, E. Schlangen, Effect of different grade levels of calcined clays on fresh and hardened properties of ternary-blended cementitious materials for 3D printing, Cem. Concr. Compos. 114 (2020), 103708, https://doi.org/10.1016/j.cemconcomp.2020.103708.

[24] D. Benkeser, K. Hernandez, F. Lolli, K. Kurtis, Influence of calcined clay morphology on flow in blended cementitious systems, Cement Concr. Res. 160 (2022), 106927, https://doi.org/10.1016/j.cemconres.2022.106927.

[25] D. Bülichen, J. Kainz, J. Plank, Working mechanism of methyl hydroxyethyl cellulose (MHEC) as water retention agent, Cement Concr. Res. 42 (2012) 953–959, https://doi.org/10.1016/j.cemconres.2012.03.016.

[26] M.A. Schultz, L.J. Struble, Use of oscillatory shear to study flow behavior of fresh cement paste, Cement Concr. Res. 23 (1993) 273–282, https://doi.org/10.1016/0008-8846(93)90092-N.

[27] Q. Yuan, D. Zhou, K.H. Khayat, D. Feys, C. Shi, On the measurement of evolution of structural build-up of cement paste with time by static yield stress test vs. small amplitude oscillatory shear test, Cement Concr. Res. 99 (2017) 183–189, https://doi.org/10.1016/j.cemconres.2017.05.014.

[28] T.G. Mezger, The Rheology Handbook, fourth ed., Emerald Group Publishing Limited, 2009 https://doi.org/10.1108/prt.2009.12938eac.006.

[29] X. Dai, S. Aydin, M.Y. Yardimci, G. De Schutter, Rheology and structural build-up of sodium silicate- and sodium hydroxide-activated GGBFS mixtures, Cem. Concr. Compos. 131 (2022), 104570, https://doi.org/10.1016/j.cemconcomp.2022.104570.

[30] N. Roussel, G. Ovarlez, S. Garrault, C. Brumaud, The origins of thixotropy of fresh cement pastes, Cement Concr. Res. 42 (2012) 148–157, https://doi.org/10.1016/j.cemconres.2011.09.004.

[31] V.N. Nerella, M.A.B. Beigh, S. Fataei, V. Mechtcherine, Strain-based approach for measuring structural build-up of cement pastes in the context of digital construction, Cement Concr. Res. 115 (2019) 530–544, https://doi.org/10.1016/j.cemconres.2018.08.003.

[32] N. Roussel, H. Bessaies-Bey, S. Kawashima, D. Marchon, K. Vasilic, R. Wolfs, Recent advances on yield stress and elasticity of fresh cement-based materials, Cement Concr. Res. 124 (2019), 105798, https://doi.org/10.1016/j.cemconres.2019.105798.

[33] S. Ma, Y. Qian, S. Kawashima, Experimental and modeling study on the non-linear structural build-up of fresh cement pastes incorporating viscosity modifying admixtures, Cement Concr. Res. 108 (2018) 1–9, https://doi.org/10.1016/j.cemconres.2018.02.022.

[34] X. Dai, S. Aydın, M.Y. Yardımcı, K. Lesage, G. De Schutter, Effects of activator properties and GGBFS/FA ratio on the structural build-up and rheology of AAC, Cement Concr. Res. 138 (2020), 106253, https://doi.org/10.1016/j.cemconres.2020.106253.

[35] D. Jiao, K. El Cheikh, C. Shi, K. Lesage, G. De Schutter, Structural build-up of cementitious paste with nano-Fe3O4 under time-varying magnetic fields, Cement Concr. Res. (2019), https://doi.org/10.1016/j.cemconres.2019.105857.

[36] X. Dai, S. Aydin, M. Yücel Yardimci, R.E.N. Qiang, K. Lesage, G. De Schutter, Rheology, early-age hydration and microstructure of alkali-activated GGBFS-Fly ash-limestone mixtures, Cem. Concr. Compos. 124 (2021), 104244, https://doi.org/10.1016/j.cemconcomp.2021.104244.

[37] Q. Yuan, X. Lu, K.H. Khayat, D. Feys, C. Shi, Small amplitude oscillatory shear technique to evaluate structural build-up of cement paste, Mater. Struct. Constr. 50 (2017) 1–12, https://doi.org/10.1617/s11527-016-0978-2.

[38] X. Dai, Q. Ren, S. Aydın, M.Y. Yardımcı, K. Lesage, G. De Schutter, Enhancing thixotropy and structural build-up of alkali-activated slag/fly ash pastes with nano clay, Mater. Struct. Constr. 54 (2021), https://doi.org/10.1617/s11527-021-01760-4.

[39] NEN-EN 196-1, Methods of Testing Cement - Part 1: Determination of Strength, 2016.
[40] O. Akhlaghi, T. Aytas, B. Tatli, D. Sezer, A. Hodaei, A. Favier, K. Scrivener, Y. Z. Menceloglu, O. Akbulut, Modified poly(carboxylate ether)-based superplasticizer for enhanced flowability of calcined clay-limestone-gypsum blended Portland cement, Cement Concr. Res. 101 (2017) 114–122, https://doi.org/10.1016/j.cemconres.2017.08.028.
[41] F. Zunino, K. Scrivener, Insights on the role of alumina content and the filler effect on the sulfate requirement of PC and blended cements, Cement Concr. Res. 160 (2022), 106929, https://doi.org/10.1016/j.cemconres.2022.106929.
[42] O. Canbek, Q. Xu, Y. Mei, N.R. Washburn, K.E. Kurtis, Predicting the rheology of limestone calcined clay cements (LC3): linking composition and hydration kinetics to yield stress through Machine Learning, Cement Concr. Res. 160 (2022), https://doi.org/10.1016/j.cemconres.2022.106925.
[43] T. Liberto, M. Bellotto, A. Robisson, Small oscillatory rheology and cementitious particle interactions, Cement Concr. Res. 157 (2022), 106790, https://doi.org/10.1016/j.cemconres.2022.106790.
[44] P. Steins, A. Poulesquen, O. Diat, F. Frizon, Structural evolution during geopolymerization from an early age to consolidated material, Langmuir 28 (2012) 8502–8510, https://doi.org/10.1021/la300868v.
[45] H.A. Barnes, Thixotropy—a review, J. Nonnewton. Fluid Mech. 70 (1997) 1–33, https://doi.org/10.1016/S0377-0257(97)00004-9.
[46] A.M. Mostafa, A. Yahia, New approach to assess build-up of cement-based suspensions, Cement Concr. Res. 85 (2016) 174–182, https://doi.org/10.1016/j.cemconres.2016.03.005.
[47] L. Nachbaur, J.C. Mutin, A. Nonat, L. Choplin, Dynamic mode rheology of cement and tricalcium silicate pastes from mixing to setting, Cement Concr. Res. 31 (2001) 183–192, https://doi.org/10.1016/S0008-8846(00)00464-6.
[48] S. Gauffinet-Garrault, The rheology of cement during setting, in: Underst. Rheol. Concr., Elsevier, 2012, pp. 96–113, https://doi.org/10.1533/9780857095282.1.96.
[49] A.M. Mostafa, A. Yahia, Physico-chemical kinetics of structural build-up of neat cement-based suspensions, Cement Concr. Res. 97 (2017) 11–27, https://doi.org/10.1016/j.cemconres.2017.03.003.
[50] P.S. de Silva, F.P. Glasser, Hydration of cements based on metakaolin: Thermochemistry, Adv. Cement Res. 3 (1990) 167–177, https://doi.org/10.1680/adcr.1990.3.12.167.
[51] F. Zunino, K. Scrivener, Factors influencing the sulfate balance in pure phase C3S/C3A systems, Cement Concr. Res. 133 (2020), 106085, https://doi.org/10.1016/j.cemconres.2020.106085.
[52] D. Marchon, R.J. Flatt, Mechanisms of Cement Hydration, Elsevier Ltd, 2015, https://doi.org/10.1016/B978-0-08-100693-1.00008-4.
[53] A. Quennoz, K.L. Scrivener, Interactions between alite and C3A-gypsum hydrations in model cements, Cement Concr. Res. 44 (2013) 46–54, https://doi.org/10.1016/j.cemconres.2012.10.018.
[54] R. Taylor, I.G. Richardson, R.M.D. Brydson, Composition and microstructure of 20-year-old ordinary Portland cement-ground granulated blast-furnace slag blends containing 0 to 100% slag, Cement Concr. Res. 40 (2010) 971–983, https://doi.org/10.1016/j.cemconres.2010.02.012.
[55] F. Bellmann, J. Stark, Activation of blast furnace slag by a new method, Cement Concr. Res. 39 (2009) 644–650, https://doi.org/10.1016/j.cemconres.2009.05.012.
[56] F. Zunino, K. Scrivener, The reaction between metakaolin and limestone and its effect in porosity refinement and mechanical properties, Cem, Concr. Res. 140 (2021), 106307, https://doi.org/10.1016/j.cemconres.2020.106307.
[57] R.J. Flatt, D. Larosa, N. Roussel, Linking yield stress measurements: spread test versus Viskomat, Cement Concr. Res. 36 (2006) 99–109, https://doi.org/10.1016/j.cemconres.2005.08.001.
[58] N. Roussel, C. Stefani, R. Leroy, From mini-cone test to Abrams cone test: measurement of cement-based materials yield stress using slump tests, Cement Concr. Res. 35 (2005) 817–822, https://doi.org/10.1016/j.cemconres.2004.07.032.
[59] H. Li, A. Wu, H. Cheng, Generalized models of slump and spread in combination for higher precision in yield stress determination, Cement Concr. Res. 159 (2022), 106863, https://doi.org/10.1016/j.cemconres.2022.106863.
[60] A. Pierre, C. Lanos, P. Estellé, Extension of spread-slump formulae for yield stress evaluation, Appl. Rheol. 23 (2013) 1–9, https://doi.org/10.3933/ApplRheol-23-63849.
[61] Y. Qian, S. Kawashima, Distinguishing dynamic and static yield stress of fresh cement mortars through thixotropy, Cem. Concr. Compos. 86 (2018) 288–296, https://doi.org/10.1016/j.cemconcomp.2017.11.019.
[62] P. Hou, T.R. Muzenda, Q. Li, H. Chen, S. Kawashima, T. Sui, H. Yong, N. Xie, X. Cheng, Mechanisms dominating thixotropy in limestone calcined clay cement (LC3), Cement Concr. Res. 140 (2021), 106316, https://doi.org/10.1016/j.cemconres.2020.106316.
[63] W.W.S. Fung, A.K.H. Kwan, Role of water film thickness in rheology of CSF mortar, Cem, Concr. Compos. 32 (2010) 255–264, https://doi.org/10.1016/j.cemconcomp.2010.01.005.
[64] N. Roussel, H. Bessaies-Bey, S. Kawashima, D. Marchon, K. Vasilic, R. Wolfs, Recent advances on yield stress and elasticity of fresh cement-based materials, Cement Concr. Res. 124 (2019), 105798, https://doi.org/10.1016/j.cemconres.2019.105798.
[65] E. Berodier, K. Scrivener, Understanding the filler effect on the nucleation and growth of C-S-H, J. Am. Ceram. Soc. 97 (2014) 3764–3773, https://doi.org/10.1111/jace.13177.
[66] L. Lei, J. Plank, A study on the impact of different clay minerals on the dispersing force of conventional and modified vinyl ether based polycarboxylate superplasticizers, Cement Concr. Res. 60 (2014) 1–10, https://doi.org/10.1016/j.cemconres.2014.02.009.
[67] E. Pustovgar, R.K. Mishra, M. Palacios, J.B. d'Espinose de Lacaillerie, T. Matschei, A.S. Andreev, H. Heinz, R. Verel, R.J. Flatt, Influence of aluminates on the hydration kinetics of tricalcium silicate, Cement Concr. Res. 100 (2017) 245–262, https://doi.org/10.1016/j.cemconres.2017.06.006.
[68] J. Lapeyre, A. Kumar, Influence of pozzolanic additives on hydration mechanisms of tricalcium silicate, J. Am. Ceram. Soc. 101 (2018) 3557–3574, https://doi.org/10.1111/jace.15518.
[69] M. Zajac, M. Wieczorek, B. Lothenbach, F. Bullerjahn, V.M. Schmidt, M. Ben, Effect of alkali and sulfate on early hydration of Portland cements at high water to cement ratio, Construct. Build. Mater. 345 (2022), 128283, https://doi.org/10.1016/j.conbuildmat.2022.128283.